Coils' Current Distortion Due to Variable Series Compensation Capacitance in EV Wireless Charging for a Constant Optimum Load

Grazian, Francesca; Shi, Wenli; Soeiro, Thiago Batista; Dong, Jianning; Bauer, Pavol

DOI
10.1109/WPW54272.2022.9854029

Publication date
2022

Document Version
Final published version

Published in
2022 Wireless Power Week, WPW 2022 - Proceedings

Coils' Current Distortion Due to Variable Series Compensation Capacitance in EV Wireless Charging for a Constant Optimum Load

Francesca Grazian, Wenli Shi, Thiago Batista Soeiro, Jianning Dong and Pavol Bauer
Delft University of Technology
Delft, The Netherlands
Email: (F.Grazian, W.Shi-3, T.BatistaSoeiro, J.Dong-4, P.Bauer)@tudelft.nl

2022 Wireless Power Week (WPW) | 978-1-6654-8445-9/22/$31.00 ©2022 IEEE | DOI: 10.1109/WPW54272.2022.9854029

***Abstract*—When considering EV wireless charging that uses inductive power transfer with magnetic resonance, the coils' current distortion must be minimized to guarantee compliance with the electromagnetic compatibility limits on the radiated magnetic field set by the relevant industrial standards. This paper analyzes the current distortion caused by switch-controlled capacitors (SCCs) used as series compensation to achieve constant optimum load (COL) matching at different coils' alignments. First, the proposed COL charging method is explained where the SCCs have either the half-wave or the full-wave modulation. Their impact on the measured coils' current distortion has been analyzed up to 30MHz by computing the fast Fourier transform (FFT). Additionally, the currents' FFT from the half-wave modulation has been compared to those resulting from the conventional series-series compensation with fixed capacitance. The SCCs using the half-wave modulation result in the highest total-lumped distortion. However, the individual amplitudes corresponding to the critical frequencies of the radiated magnetic field's limit from SAE J2954 are comparable or lower than those resulting from the other implementations. Finally, the radiated magnetic field resulting from each strategy has been evaluated using the finite element method. All results are well within the SAE J2954 recommended limits at 10 m. Moreover, a minimum distance of 25 cm from the outer sides of the coupled coils ensures a safe exposure to both the general public and implanted medical devices according to the ICNIRP reference levels.**

***Index Terms*—Current distortion, electric vehicles, fast Fourier transform, switch-control capacitance, wireless charging.**

I. Introduction

Inductive power transfer (IPT) with magnetic resonance coupling is mostly used in wireless charging of electric vehicles (EVs). As a demonstration of that, there are several companies that already propose these products on the market, such as: WiTricity, IPT Group, Plugless Power, Momentum Dynamics and ElectReon. These IPT systems consist of resonant circuits with one or more sets of coupled coils which air gap is generally equal or grater that $100\,\mathrm{mm}$. This results in the coils' mutual inductance being considerably lower than their self-inductance. Moreover, the mutual inductance is generally variable because the distance between the coils varies depending on the EV position in a parking spot.

EV wireless charging solutions have essentially two main challenges. First, ensuring a highly efficient power transfer throughout the whole EV battery charging profile at different coils' alignments. Second, guaranteeing that the radiated magnetic field is not harmful to the living beings in the surroundings and is lower than the recommended EMC limits.

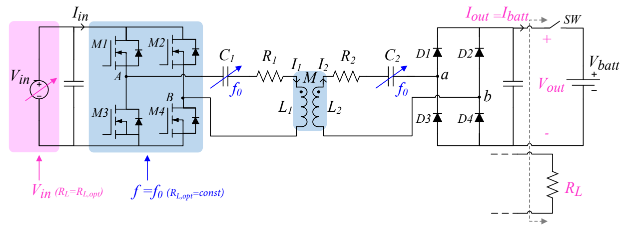

Fig. 1. Equivalent circuit of the IPT system that uses the proposed constant optimum load charging strategy with variable series compensation.

Several researches have demonstrated that employing switch-controlled capacitors (SCCs) in the compensation network can improve the power transfer efficiency of the IPT system. In [1]–[4], the SCC has been used such that the constant operating frequency matches the resonant frequency as the self-inductance of the coils changes with the misalignment.

However, it is interesting to evaluate the impact of the SCCs on the coils' current distortion since it would influence the radiated magnetic field in the radio frequency spectrum that is well-regulated by the EMC standards. This analysis is fundamental to allow the use of active compensation components such as SCCs in commercial EV wireless charging products.

On that purpose, this paper analyzes the current distortion caused by the SCCs used as series compensation to achieve constant optimum load (COL) matching at different coils' alignments. In particular, two SCC implementations have been adopted: the half-wave and the full-wave modulation. The COL battery charging strategy and the SCC implementations are explained in Section II. The fast Fourier transform (FFT) of the measured primary coil's current has been computed and analyzed in Section III for the worst operating condition. The effect of the two SCC modulations are evaluated up to $30\,\mathrm{MHz}$. Moreover, the current distortion due to the SCC half-wave modulation is compared to the one resulting from a standard fixed series compensation for the same operating conditions. In Section IV, the radiated magnetic field generated by each strategy is evaluated through the finite element method (FEM) at $10\,\mathrm{m}$ and compared to the recommended limits from the SAE J2954. After that, the radiated magnetic field in the close surrounding of the coupled coils is compared to the human exposure limits from ICNIRP Guideline 2010. Finally, the main conclusions are listed in Section V.

II. COL through variable series compensation

As explained in [5]–[7], high efficiency power transfer is achieved when using the series-series (S-S) compensation

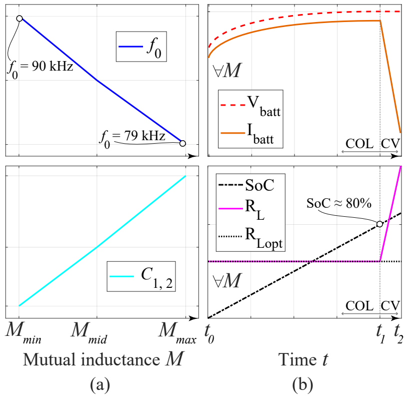

Fig. 2. Concept of the COL charging strategy. (a) Selection of the resonant frequency f_0 and compensation capacitance $C_{1,2}$ depending on the mutual inductance M. (b) Output parameters during one battery charging cycle.

network if the equivalent resistive load $R_L = \frac{V_{out}}{I_{out}}$ matches the value $R_{L,opt}$ in (1), defined as the equivalent optimum load.

$$R_{L,opt} = \frac{\pi^2}{8} \omega_0 M \sqrt{\frac{R_2}{R_1}} \tag{1}$$

Since (1) is dependent on the mutual inductance M, the optimum load condition varies with the coils' alignment. In the literature [3], [5], [6], this issue has been resolved by an additional dc-dc converter with the function to regulate the equivalent resistive load seen by the resonant circuit to always match (1) through the control of this circuit output voltage. Conversely, this paper proposes the COL that keeps $R_{L,opt}$ constant by varying the circuit's resonant frequency $f_0 = \frac{\omega_0}{2\pi}$ to counteract the changes in M. Since $R_{L,opt}$ is kept constant, there is no need for the auxiliary dc-dc converter to provide the resonant circuit output voltage control.

According to SAE J2954 [8], the operating frequency of the IPT systems for EV wireless charging is limited to the range that goes from 79 kHz to 90 kHz. This restricts the range of M for which $R_{L,opt}$ can be kept constant. For this reason, the COL strategy is more suitable for static EV wireless charging where the coils' alignment is confined. The proposed COL charging method is shown in Fig. 2(a). The IPT system's resonant frequency f_0 is selected based on the value of M resulting in the choice of the compensation capacitance.

During one battery charging cycle, the COL mode replaces the traditional constant current (CC) mode to ensure that $R_L = R_{L,opt}$ while the battery voltage increases. This means that the output current should increase proportionally with the battery voltage. Since in the S-S compensation operates close to a current source with $I_{batt} \approx \frac{2}{\pi} \frac{V_{in}}{\omega_0 M}$, the output current can be regulated by controlling V_{in} as shown in Fig. 1, which can be realized through a boost-like power factor converter (PFC) employed for the grid connection. A qualitative example of the COL is shown in Fig. 2(b) for a battery charging profile which is valid for any value of M in the permitted range $[M_{min}, M_{max}]$ from Fig. 2(a).

A. Implementation of the variable compensation capacitance

The variable compensation capacitance in Fig. 1 has been realized as SCC. Depending on the number of used semiconductor devices, there are two possible implementations: the

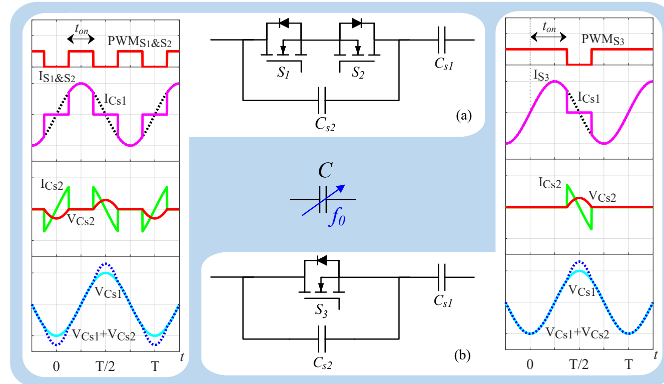

Fig. 3. Implementation of variable capacitors as switch-control capacitor (SCC) with: (a) full-wave and (b) half-wave modulation.

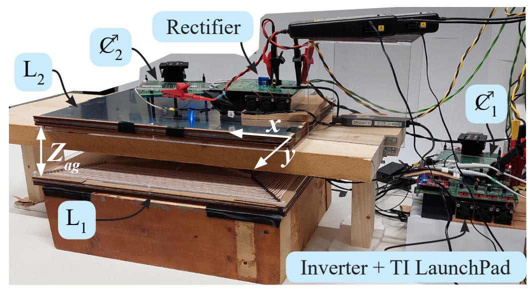

Fig. 4. Prototype of the 3.7 kW EV wireless charging system.

TABLE I

CIRCUIT PARAMETERS AND DEVICES USED IN THE PROTOTYPE OF FIG. 4.

V_{out} (V)	317...410	**Devices**	M1...M4	C2M0040120D
I_{out}: CC, COL (A)	7, 7.48		D1...D4	C4D15120D
V_{in} (V)	360...515		S1...S3	C2M0045170P
f_0 (kHz)	79...90		C unit	B32671L
L_1, L_2 (µH)	336.9, 224.2		M_{min}, M_{mid}	90.1, 95.4
C_{s1_1}, C_{s1_2} (nF)	13.50, 18.57		M_{max} (µH)	102.6
C_{s2_1}, C_{s2_2} (nF)	28.03, 52.08		C_1, C_2 (nF)	15.14, 18.55

full-wave modulation in Fig. 3(a) and the half-wave modulation in Fig. 3(b). In both cases, the value of the equivalent capacitance ranges from $\frac{C_{s1}C_{s2}}{C_{s1}+C_{s2}}$ to C_{s1} depending on the duty cycle x=$\frac{t_{on}}{T}$ of the SCC, where x=$[0...\frac{1}{2}]$. In particular, the variation of capacitance is described in (2) and (3) for the full-wave and the half-wave modulation, respectively.

The main difference between the two SCC implementations is that the full-wave modulation has additional conduction and switching losses since it employs one extra MOSFET than in the half-wave modulation case. On the other hand, for the same C_{s1}, C_{s2} and current conditions, the MOSFET in the half-wave modulation has to stand double of the blocking voltage.

$$C_{\text{f-w}} = \frac{1}{\frac{1}{C_{s1}} + \frac{1}{C_{s2}} \left(\frac{\pi - 2\pi\text{x} - \sin 2\pi\text{x}}{\pi} \right)} \tag{2}$$

$$C_{\text{h-w}} = \frac{1}{\frac{1}{C_{s1}} + \frac{1}{C_{s2}} \left(\frac{2\pi - 4\pi\text{x} + \sin 4\pi\text{x}}{2\pi} \right)} \tag{3}$$

B. Laboratory prototype and measurements

The 3.7 kW EV wireless charging system in Fig. 4 has been implemented to prove the COL charging strategy. The circuit paramenters and components used are listed in Table I. The measured circuit waveforms are shown in Fig. 5 for the two SCC modulations at three points of coils' alignment.

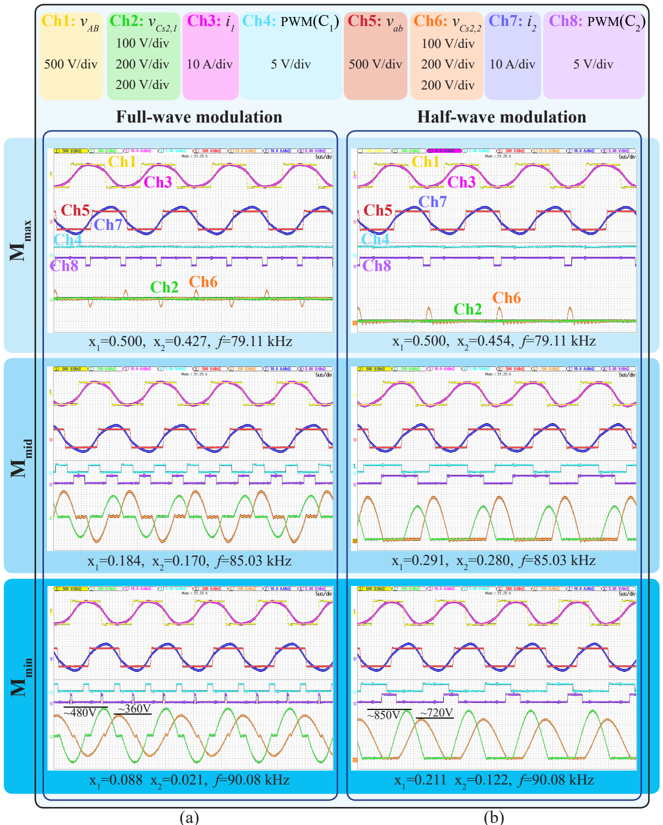

Fig. 5. Waveforms at different coils' alignments of the proposed COL by using the SCCs with (a) full-wave and (b) half-wave modulations. These waveforms have been measured at full power (V_{out}=410 V, I_{out}=7.48 A).

The half-wave modulation results in higher power transfer efficiency because of the lower power losses in the SCCs. However, it is interesting to evaluate how the two SCC implementations impact the current distortion.

III. Measured currents' distortion

Intuitively, the SCCs connected in series with the coupled coils would introduce some distortion in the coils' current. According to Fig. 5, the full-wave modulation introduces symmetrical distortions while the half-wave modulation introduces asymmetrical distortions due to their nature. Higher frequency current harmonics potentially can radiate a magnetic field which must be within the recommended limit from SAE J2954 in Fig. 6 defined for wireless charging of light-duty EVs. During the preliminary research stage, it is reasonable to conduct a qualitative and comparative analysis on the coils' current distortion rather than considering the radiated magnetic field. This investigation cannot guarantee compliance to the recommended limits, but it can preliminary assess the impact of the proposed method on the currents' higher-order harmonics. All in all, this section qualitatively analyzes and compares the FFT of the measured coils' current that result from the SCC half-wave and full-wave modulations, and the conventional S-S compensation. After that, the FEM analysis of the radiated magnetic field is performed in Section IV.

A. Methodology

1) Current measurement conditions: When measuring the circuit waveforms at the operating points shown in Fig. 5, another set of measurements of I_1 and I_2 has been performed with 50 MHz N2782B Keysight current probes such that the signals are acquired with the maximum vertical resolution. The horizontal scale of 2 ms/div is chosen that makes the measurement duration D=20 ms. A whole number of periods of the measured signals has been considered to compute the currents' FFT. These scope settings resulted in a length of the signal L=$12.5{\cdot}10^6$. Therefore, for each measured signal, the sampling period and the sampling frequency are h_{res}=$\frac{\mathrm{D}}{\mathrm{L}}$=1.6 ns and F_s=$\frac{1}{h_{res}}$=625 MHz, respectively. According to the Nyquist-Shannon sampling theorem, the FFT bandwidth f_n=$\frac{F_s}{2}$=312.5 MHz is large enough for the upper frequency limit (30 MHz) in Fig. 6. Additionally, the FFT frequency resolution is df=$\frac{F_s}{L}$=50 Hz which is reasonably small compared to the current's fundamental frequency ($\sim$ 85 kHz).

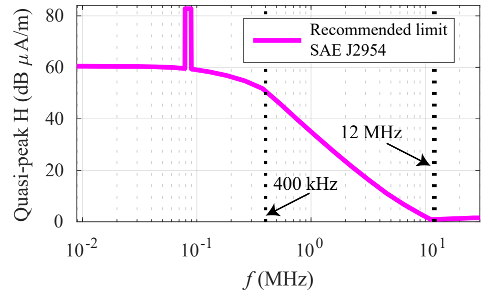

Fig. 6. Recommended limit from SAE J2954 on the quasi-peak radiated magnetic field H measured at 10 m distance [8].

TABLE II
THD of the measured I_1 and I_2 at the rated output power for different coils' alignment conditions.

	THD(I_1) (%)			THD(I_2) (%)		
	M_{min}	M_{mid}	M_{max}	M_{min}	M_{mid}	M_{max}
SCC: f-w	6.84	7.83	7.28	7.11	8.38	8.14
SCC: h-w	7.89	10.57	7.37	7.36	10.98	8.16
const C	6.16	6.65	7.69	8.16	8.51	9.04

2) Chosen operating condition: For each implementation, the total harmonic distortion (THD) of both I_1 and I_2 has been computed, which are listed in Table II for all the considered coils' alignments. However, it is more significant to discuss the amplitude of individual harmonics rather than the THD since those determine the compliance to the limits in Fig. 6. It is worth mentioning that this limit drops exponentially from 400 kHz to 12 MHz where the minimum value is reached, and it is roughly maintained constant until 30 MHz. The peak amplitude of the harmonic components has been considered since it coincides with the quasi-peak value in continuous wave signals. Nevertheless, the quasi-peak is always equal or lower than the relative peak and, for this reason, the peak normally gives an extra safety margin.

In the following analysis, the middle-point coil's alignment M=M_{mid} is considered since it leads to the highest distortion due to the SCCs switching at relatively high currents as shown in Fig. 5. Only I_1 is discussed in detail since, according to Fig. 7, larger distortions have been found at the primary circuit due to the band-pass filter characteristic of the resonant network as explained in [9]. Fig. 8 shows the FTT I_1 resulting from the SCC half-wave and full-wave modulations measured at

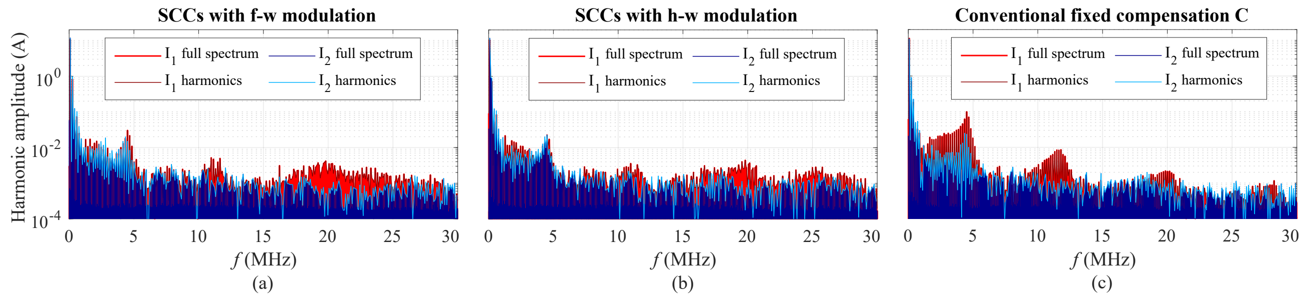

Fig. 7. FFT of I_1 and I_2 at the maximum power point for M=M_{mid} when using: (a) SCCs with full-wave (f-w) modulation, (b) SCCs with half-wave (h-w) modulation, and (c) fixed S-S compensation (const C). The FTT is plotted for the entire frequency spectrum and also for only the harmonic components.

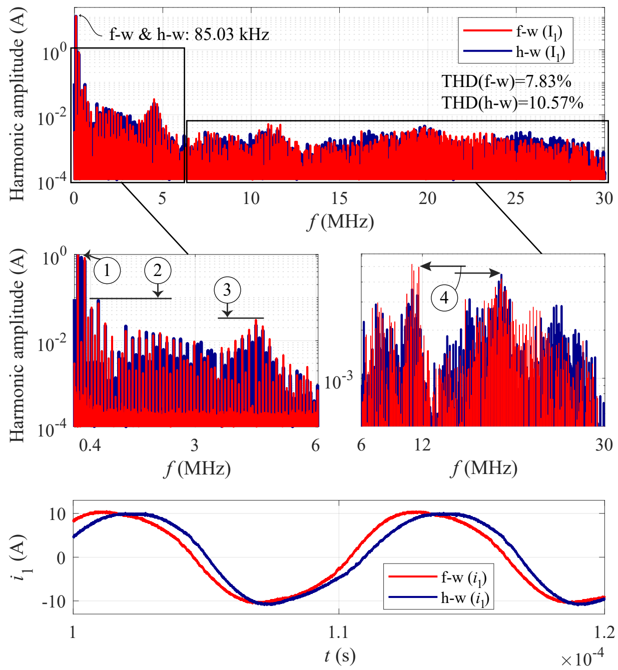

Fig. 8. FFT of I_1 at full power for M=M_{mid} when using SCCs with full-wave (f-w) and half-wave (h-w) modulations.

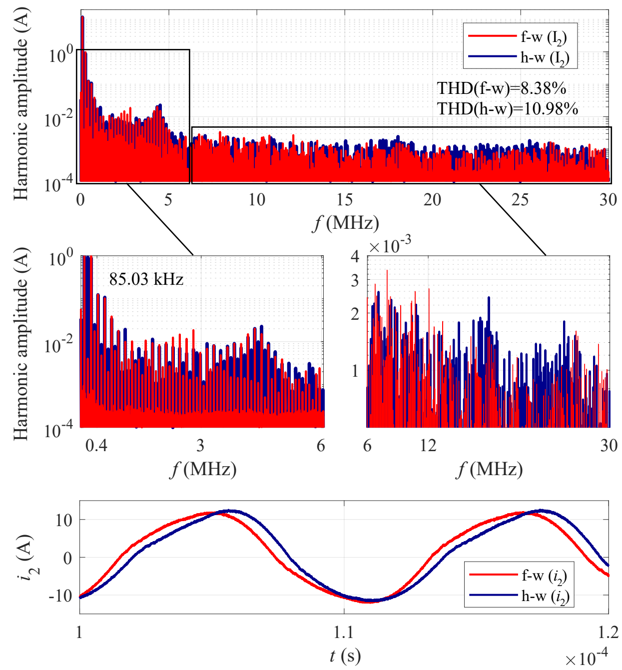

Fig. 9. FFT of I_2 at full power for M=M_{mid} when using SCCs with full-wave (f-w) and half-wave (h-w) modulations.

M=M_{mid}. The FFT of the respective I_2 is shown in Fig. 9. On the other hand, Fig. 10 shows the FTT of I_1 resulting from the SCC half-wave modulation and the compensation with fixed capacitors both measured at M=M_{mid}. The FFT of the respective I_2 is shown in Fig. 11.

B. SCCs using the half-wave and the full-wave modulations

From the lower-frequencies zoom of Fig. 8, the half-wave modulation has more significant even-order harmonic components than the full-wave modulation due to its asymmetrical nature. This can be seen especially in the 2^{nd}-order harmonic highlighted by (1). This 2^{nd}-order harmonic might not be particularly worrying because it would not be likely the only one compromising the compliance since its amplitude is similar to the 3^{rd}-harmonic from the full-wave modulation. Similarly, the half-wave modulation's 7^{th}-order harmonic (595 kHz) pointed out from (2) is about 2.8 times higher than the full-wave modulation's 53^{th}-order harmonic (4.5 MHz) marked by (3). Nevertheless, according to Fig. 6, the limit at 595 kHz is about 25 times lager than the one at 4.5 MHz.

Considering the zoom on the highest frequencies of Fig. 8, it is clear from (4) that the full-wave modulation has the most compromising harmonic amplitude in the range of 12-30 MHz.

From this analysis, it can be concluded that the half-wave modulation leads to more total-lumped distortion in I_1 which is confirmed by the THD. However, since the harmonic components have comparable amplitude, it cannot be stated that one specific modulation strategy would be compromising the recommended limits more than the other. Similar considerations are also valid for the harmonic distortion of the respective measured I_2 shown in Fig. 9.

C. Half-wave modulation SCC and the fixed S-S capacitors

In the lower-frequencies zoom of Fig. 10, it is possible to notice that the half-wave modulation has larger even-order harmonic components due to its asymmetrical nature. However, similarly to the previous analysis, the 2^{nd}-order harmonic highlighted from (1) might not be particularly worrying. After this, it is interesting to notice that the largest amplitudes in the interval from 400 kHz to 12 MHz are generated by the compensation with fixed capacitors, marked by (2) and (3).

Considering the zoom on the highest frequencies of Fig. 10, it is clear at (4) that the fixed capacitors lead to compromising harmonic amplitudes also in the range 12-30 MHz. This high-frequency ringing visible in the measured signal is due to the parasitic capacitance of the coil. This ringing might be less

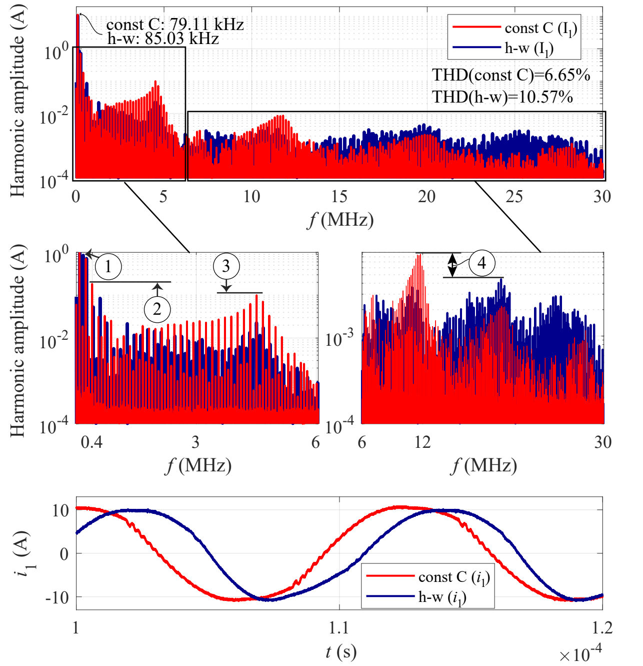

Fig. 10. FFT of I_1 at full power for M=M_{mid} when using the fixed S-S compensation (const C), and the SSC half-wave (h-w) modulation.

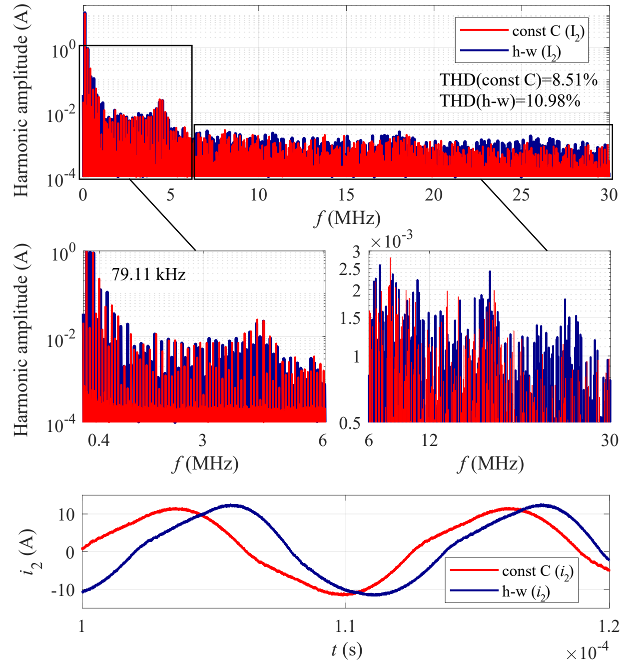

Fig. 11. FFT of I_2 at full power for M=M_{mid} when using the fixed S-S compensation (const C), and the SSC half-wave (h-w) modulation.

attenuated when using fixed capacitors because the resistance of the resonant circuit is lower than in the implementations with SCCs. This reduces the conduction losses but it worsen the dumping of the high-frequency oscillations.

The half-wave modulation leads to higher total-lumped distortion in I_1. However, considering that the compensation with fixed capacitors leads to larger amplitudes of the harmonic components at the most stringent limits, it can be deduced that if the latter complies with the recommended limits also the implementation with SCCs using half-wave modulation would. Similar considerations are also valid for the harmonic distortion of the respective measured I_2 shown in Fig. 11.

IV. FEM SIMULATION OF THE RADIATED MAGNETIC FIELD

After the analysis of the current distortion, it is interesting to evaluate whether the radiated magnetic field generated by these currents is below the EMC limits in Fig. 6. For that purpose, the coils in Fig. 4 have been modelled in Comsol Multiphysics for the alignment condition corresponding to M_{mid} where the assigned I_1 and I_2 have harmonic components equal to the measured ones in amplitude and phase. According to Fig. 7, it is reasonable to consider only the higher-order harmonic components instead of the full spectrum since the peaks occur in correspondence of those. The radiated magnetic field has been evaluated through the FEM analysis for each configuration in Fig. 7. To ensure accuracy of the solutions at $10\,\mathrm{m}$, the infinite element domain is applied to the external layer of the air domain shown in Fig. 12 [10]. All evaluations points are shown in Fig. 13 of which height is z=$\frac{Z_{ag}}{2}$. This is a conservative analysis since the receiver coil is not provided of a large aluminum shield resembling the EV chassis.

A. Comparison with the EMC limits

Fig. 14 shows the comparison between the radiated magnetic field and the recommended limits from SAE J2954 in

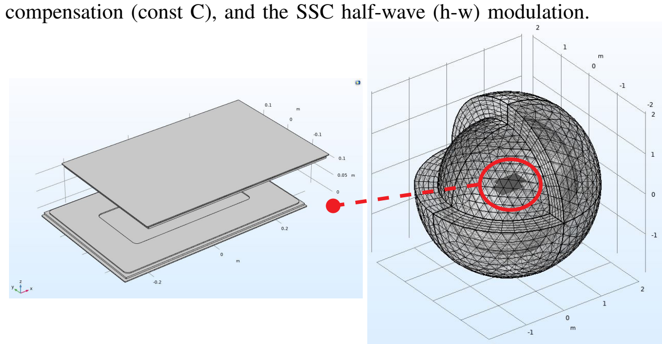

Fig. 12. Model of the coupled coils to evaluate the radiated magnetic field.

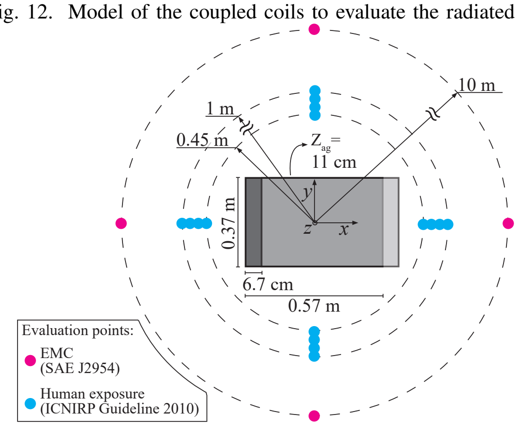

Fig. 13. Locations of the evaluated radiated magnetic field for lateral misalignment of the receiver coil in the x direction corresponding to M_{mid}.

the four $10\,\mathrm{m}$-distant points illustrated in Fig. 13. The resulting B_{peak} has been converted by using (4).

$$\overbrace{H_{peak}}^{(dB_{\mu A/m})} = 20 \cdot \log_{10}\left[\overbrace{\frac{B_{peak}}{\mu_0}}^{(T)} \cdot 10^6\right] \qquad (4)$$

The radiated field is well below the limits as expected since

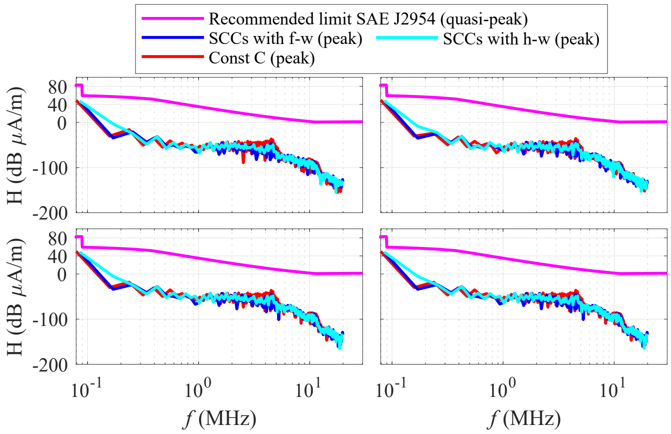

Fig. 14. Computed radiated magnetic field at 10 m.

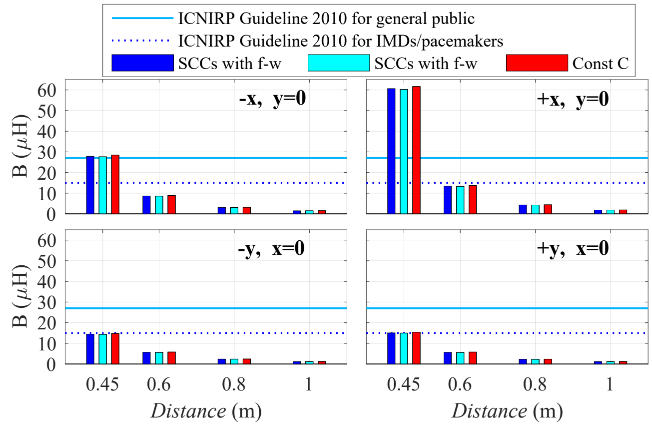

Fig. 15. Computed radiated magnetic field within 1 m.

the considered power level of 3.7 kW is the lowest regulated by SAE J2954. A radiated B_{peak} up to 43 times larger than the maximum resulting one of 50 dB would still satisfy the limit in the nominal operating frequency range 79-90 kHz. Thereby, SAE J2954 also suggests reducing the limit by 15 dB if sensitive equipment is present within 10 m. In that case, the radiated B_{peak} can be up to 7 times larger.

B. Comparison with the human exposure limits

Besides the compliance to the EMC limits, the magnetic field radiated by the coupled coils must be safe for the living beings in the surrounding of the EV wireless charging system. The ICNIRP Guideline 2010 defines reference levels for the general public exposure being B_{rms}=27 µT, while the limit B_{rms}=15 µT holds for implanted medical devices (IMDs) and pacemakers [11]. These limits are valid for all the areas around the IPT system accessible to people.

Fig. 15 shows the evaluated radiated magnetic field in the four directions specified in Fig. 13. It can be deduced that, in this case, a minimum distance of 25 cm from the outer sides of the coupled coils guarantees a radiated $B_{rms} \leq 15$ µT. When considering the wireless charging system mounted on the EV, the EV chassis can provide easily this safety distance.

V. Conclusion

This paper analyzes the current distortion introduced by using switched controlled capacitors or SCCs as series compensation. This is important to preliminary assess the radiated magnetic field in the higher frequency domain. The SCCs are employed to change the circuit's resonant frequency such that the optimum load condition is kept constant over different coils' alignments. The coils' current has been measured in a 3.7kW EV wireless charging system for three implementations: SCCs with half-wave modulation, SCCs with full-wave modulation, and conventional fixed capacitance. By computing the current's FFT up to 30MHz, the SCCs using the half-wave modulation introduce the highest total lumped distortion because of their asymmetrical nature. However, in correspondence with the critical frequencies of the limits set by SAE J2954, the amplitude of the single harmonic components are comparable or lower than in the other implementations. After that, the radiated magnetic field from each configuration was evaluated through FEM analysis. The results at 10 m distance are all far below the EMC limits from SAE J2954 up to 30 MHz. When considering the human exposure limits set by ICNIRP, a minimum distance of 25 cm from the outer sides of the coupled coils ensures a safe magnetic field level for both the general public and implanted medical devices.

References

[1] J. Osawa, T. Isobe, and H. Tadano, "Efficiency improvement of high frequency inverter for wireless power transfer system using a series reactive power compensator," in *2017 IEEE 12th International Conference on Power Electronics and Drive Systems (PEDS)*, 2017, pp. 992–998.

[2] D. Kim and D. Ahn, "Self-tuning lcc inverter using pwm-controlled switched capacitor for inductive wireless power transfer," *IEEE Transactions on Industrial Electronics*, vol. 66, no. 5, pp. 3983–3992, 2019.

[3] J. Zhang, J. Zhao, Y. Zhang, and F. Deng, "A wireless power transfer system with dual switch-controlled capacitors for efficiency optimization," *IEEE Transactions on Power Electronics*, vol. 35, no. 6, 2020.

[4] W. Li, G. Wei, C. Cui, X. Zhang, and Q. Zhang, "A double-side self-tuning lcc/s system using a variable switched capacitor based on parameter recognition," *IEEE Transactions on Industrial Electronics*, vol. 68, no. 4, pp. 3069–3078, 2021.

[5] R. Bosshard, J. W. Kolar, J. Mühlethaler, I. Stevanovic, B. Wunsch, and F. Canales, "Modeling and η-α-pareto optimization of inductive power transfer coils for electric vehicles," *IEEE Journal of Emerging and Selected Topics in Power Electronics*, vol. 3, pp. 50 – 64, 2015.

[6] S. Bandyopadhyay, P. Venugopal, J. Dong, and P. Bauer, "Comparison of magnetic couplers for ipt-based ev charging using multi-objective optimization," *IEEE Transactions on Vehicular Technology*, vol. 68, no. 6, pp. 5416–5429, 2019.

[7] F. Grazian, W. Shi, T. B. Soeiro, J. Dong, and P. Bauer, "Electric vehicle charging based on inductive power transfer employing variable compensation capacitance for optimum load matching," in *IECON 2020 The 46th Annual Conference of the IEEE Industrial Electronics Society*, 2020, pp. 5262–5267.

[8] *J2954 (R) Wireless Power Transfer for Light-Duty Plug-In/ Electric Vehicles and Alignment Methodology*, SAE International Std., Oct. 2020.

[9] H. Zeng, S. Yang, and F. Z. Peng, "Design consideration and comparison of wireless power transfer via harmonic current for phev and ev wireless charging," *IEEE Transactions on Power Electronics*, vol. 32, no. 8, 2017.

[10] W. Shi, F. Grazian, J. Dong, T. B. Soeiro, and P. Bauer, "Analysis of magnetic field emissions in inductive power transfer ev chargers following reference designs in sae j2954/2019," in *2020 IEEE International Symposium on Circuits and Systems (ISCAS)*, 2020, pp. 1–5.

[11] *ICNIRP Guidelines for limiting exposure to time-varying electric and magnetic fields (1Hz - 100 kHz)*, Health Physics 99(6):818-836, International Commission on Non-Ionizing Radiation Protection Std., 2010.